High-Resolution Soft X-ray Photoelectron Spectroscopic Studies and Scanning Auger Microscopy Studies of the Air Oxidation of Alkylated Silicon(111) Surfaces

Lauren J. Webb,[†] David J. Michalak,[†] Julie S. Biteen,[†] Bruce S. Brunschwig,[†] Ally S. Y. Chan,[‡] David W. Knapp,[†] Harry M. Meyer, III,[§] Eric J. Nemanick,[†] Matthew C. Traub,[†] and Nathan S. Lewis*,[†]

Division of Chemistry and Chemical Engineering, California Institute of Technology, 210 Noyes Laboratory, 127-72, Pasadena, California 91125, Department of Physics and Astronomy and Laboratory for Surface Modification, Rutgers University, Piscataway, New Jersey 08854, and High-Temperature Materials Laboratory, Oak Ridge National Laboratory, Oak Ridge, Tennessee 37831

Received: May 31, 2006

High-resolution soft X-ray photoelectron spectroscopy was used to investigate the oxidation of alkylated silicon(111) surfaces under ambient conditions. Silicon(111) surfaces were functionalized through a two-step route involving radical chlorination of the H-terminated surface followed by alkylation with alkylmagnesium halide reagents. After 24 h in air, surface species representing Si^{+}, Si^{2+}, Si^{3+}, and Si^{4+} were detected on the Cl-terminated surface, with the highest oxidation state (Si^{4+}) oxide signal appearing at +3.79 eV higher in energy than the bulk Si $2p_{3/2}$ peak. The growth of silicon oxide was accompanied by a reduction in the surface-bound Cl signal. After 48 h of exposure to air, the Cl-terminated Si(111) surface exhibited 3.63 equivalent monolyers (ML) of silicon oxides. In contrast, after exposure to air for 48 h, CH_3-, C_2H_5-, or $C_6H_5CH_2$-terminated Si surfaces displayed <0.4 ML of surface oxide, and in most cases only displayed ≈0.20 ML of oxide. This oxide was principally composed of Si^{+} and Si^{3+} species with peaks centered at +0.8 and +3.2 eV above the bulk Si $2p_{3/2}$ peak, respectively. The silicon 2p SXPS peaks that have previously been assigned to surface Si−C bonds did not change significantly, either in binding energy or in relative intensity, during such air exposure. Use of a high miscut-angle surface (7° vs ≤0.5° off of the (111) surface orientation) yielded no increase in the rate of oxidation nor change in binding energy of the resultant oxide that formed on the alkylated Si surfaces. Scanning Auger microscopy indicated that the alkylated surfaces formed oxide in isolated, inhomogeneous patches on the surface.

I. Introduction

The H-terminated crystalline Si(111) surface has been well-documented to have a low surface recombination velocity.[1,2] However, this surface oxidizes rapidly in ambient air, resulting in a surface that has a high surface recombination velocity.[1] A variety of surface passivation schemes have been investigated with the aim of preserving the ideal electrical and electronic properties of the H-terminated Si(111) surface in ambient conditions.[3]

One promising technique involves the formation of Si−C bonds to the atop Si sites on the Si(111) surface.[3] Extensive work in our laboratory has focused on the use of a two-step chlorination/alkylation procedure to produce well-defined, alkylated Si surfaces.[4,5] Such surfaces have been shown to exhibit very low surface recombination velocities, indicating relatively few electrically active defect sites on the functionalized surface.[1,5] Consistently, no silicon oxides are detectable by surface-sensitive X-ray photoelectron spectroscopy on such initially prepared alkylated Si surfaces.[4,5] Although the rate of oxidation is significantly impeded, core-level photoelectron spectroscopy of the Si 2p region has shown that the alkylated Si(111) surfaces show small but detectable levels of oxide after several weeks of air exposure.[5] However, the alkylated Si(111) surfaces still show low surface recombination velocities after this time period.[1,5] A question of interest is therefore the nature of the oxide that is formed on these surfaces as compared to the electrically defective oxide that forms during air oxidation of H-terminated Si(111) surfaces.

To address this issue, we have used high-resolution, "soft" X-ray photoelectron spectroscopy (SXPS) to investigate the oxidation of Si(111) surfaces alkylated with CH_3−, C_2H_5−, and C_6H_5-CH_2− groups. The high resolution of the synchrotron light source provides enhanced spectroscopic information on the oxidation state of the species on the Si surface, and the soft X-ray photon energy allows generation of Si 2p photoelectrons that have low escape depths, providing enhanced surface sensitivity over what is typically possible with traditional X-ray generation sources in laboratory-based XPS instruments. To determine the importance of step edge-mediated oxidation processes, the oxidation of alkylated Si surfaces having varying densities of surface step edges was investigated by increasing the miscut angle of the surface from the (111) orientation. Additionally, scanning Auger microscopy (SAM) was used to measure the spatial patterns of oxide growth on the alkylated Si(111) surfaces.

II. Experimental Section

A. Materials and Methods. *1. Materials.* For core photoelectron studies, 525 μm thick silicon(111) wafers polished on

* To whom correspondence should be addressed.
[†] California Institute of Technology.
[‡] Rutgers University.
[§] Oak Ridge National Laboratory.

10.1021/jp063366s CCC: $33.50 © 2006 American Chemical Society
Published on Web 10/31/2006

one side were obtained from Crysteco (Wilmington, OH). These n-type samples were doped with P to a resistivity of 2−8.5 Ω cm. To study the effect of step edge density on the air oxidation of alkylated surfaces, Sb-doped, 0.005−0.02 Ω cm resistivity, n-type Si(111) wafers with a miscut angle of ±0.5° were obtained from ITME (Poland). Additionally, stepped P-doped n-type Si(111) wafers with a resistivity of 0.005−0.02 Ω cm and a miscut angle of 7° were obtained from Montco Silicon Technologies (Spring City, PA).

All solvents used in the alkylation reactions were anhydrous, stored under N_2(g), and were used as received from Aldrich Chemical Corp. The solvents were only exposed to the atmosphere of a N_2(g)-purged flush box. Nanopure H_2O with a resistivity >17.8 MΩ cm was used at all times. All other chemicals were used as received.

2. Sample Preparation. Before functionalization, each Si sample was cleaned by sequential immersion for 3 s each in a sonicated bath of CH_3OH, acetone, CH_2Cl_2, 1,1,1-trichloroethane (TCE), CH_2Cl_2, acetone, and CH_3OH. The sample was then subjected to a final rinse with H_2O. Occasionally a different cleaning procedure was used in which the sample was rinsed in a flowing stream of H_2O, CH_3OH, acetone, CH_3OH, and H_2O, then dried under a stream of N_2(g). After cleaning by either method, the sample was placed directly in 40% NH_4F(aq) (Transene, Inc.) for 20 min to etch away the native oxide layer and produce a H-terminated Si(111) surface. During the etching process, the wafers were occasionally agitated to remove the bubbles that formed on the surface. After removal from the etching solution, the sample was rinsed thoroughly with H_2O and dried under a stream of N_2(g). The sample was then either introduced into a quick-entry chamber of the ultra-high vacuum (UHV) system for XPS or SXPS analysis or was placed into the antechamber of a N_2(g)-purged glovebox for further functionalization.

Hydrogen-terminated Si(111) surfaces were chlorinated according to previously published procedures.[4,5] A freshly etched surface was first immersed in a saturated solution of PCl_5 (99.998%, Alfa Aesar) in chlorobenzene to which a few grains of benzoyl peroxide had been added. The reaction solution was then heated to 90−100 °C for 45 min. The sample was then removed from the reaction solution, and rinsed with tetrahydrofuran (THF), CH_3OH, and again with THF, after which the THF was allowed to evaporate quickly from the sample surface. X-ray photoelectron spectra of the Cl-terminated surface were collected, after which the sample was removed from the UHV system, exposed to ambient air and lighting conditions in the laboratory, and periodically returned to UHV for additional analysis by SXPS.

To alkylate the Si surface, the Cl-terminated Si(111) sample was immersed in a 1.0−3.0 M solution of $C_nH_{2n+1}MgX$ (n = 1, 2 and X = Cl or Br (Aldrich)) in THF. Samples were additionally functionalized by immersion in a 2.0 M solution of $C_6H_5CH_2MgCl$ in THF (Aldrich). Excess THF was added to each reaction solution to compensate for the loss of solvent through evaporation. This solution was heated at 70−80 °C for 3−4 h for n = 1; for 5 h for n = 2; and for 16−18 h for functionalization with $C_6H_5CH_2$−. At the end of the reaction, the sample was removed from the alkylmagnesium solution, rinsed with copious amounts of THF and CH_3OH, immersed in CH_3OH, and removed from the N_2(g)-purged glovebox. The sample was sonicated for 5 min in CH_3OH, sonicated in CH_3CN for a further 5 min, and then dried under a stream of N_2(g). The alkyl-terminated sample was then introduced into the quick-entry load lock of the UHV chamber for core photoelectron spectroscopic analysis. After spectra of the freshly prepared surface had been collected, the samples were removed from the UHV system and were exposed to ambient air and light conditions to allow growth of Si oxides. The samples were periodically examined by SXPS to follow the growth of such oxides.

B. Instrumentation. *1. SXPS Measurements.* High-resolution SXPS experiments were performed on beamline U4A at the National Synchrotron Light Source (NSLS) at Brookhaven National Laboratory.[6] The sample was introduced through a quick-entry load lock into a two-stage UHV system that was maintained at pressures $\leq 1 \times 10^{-9}$ Torr. The beamline had a spherical grating monochromator that selected photon energies between 10 and 300 eV with a resolution of 0.1 eV. The selected excitation energy was not calibrated independently because our study was principally concerned with shifts in the Si 2p binding energy in reference to the bulk Si 2p peak, as opposed to the determination of absolute binding energies. Hence any relatively small energy peak shifts could be due to a slight change in energy of the excitation beam with time, as opposed to an actual shift in the energy of the peaks on the samples. Samples were illuminated at an incident energy of 140 eV, and the emitted photoelectrons were collected by a VSW 100 mm hemispherical analyzer that was fixed at 45° off the axis of the photon source and 90° off of the sample surface. The beam intensity from the synchrotron ring was measured independently, and the data in each scan were normalized to account for changes in photon flux during the scan. No charging was observed on the samples during data collection. The limited range of excitation energies available at this beamline, although well-suited for high surface resolution Si 2p core level spectroscopy, precluded collection of survey scans that would have identified other atomic species present on the Si surface.

The escape depth of Si 2p photoelectrons was calculated by using a method described by Seah.[7] The size of the Si atom, a_{Si}, was determined with eq 1:

$$a_{Si} = \left(\frac{A_{Si}}{\rho_{Si} N_A}\right)^{1/3} \quad (1)$$

where A_{Si} is the atomic weight of Si (28.086 g mol^{-1}), ρ_{Si} is the density of the crystal (2.328 g cm^{-3}),[8] and N_A is Avogadro's number, yielding a_{Si} = 0.272 nm. The electron mean free path, λ_{Si}, was then calculated from the empirical relation:[7]

$$\lambda_{Si} = (0.41\ \mathrm{nm}^{-1/2}\ \mathrm{eV}^{-1/2}) a_{Si}^{1.5} E_{Si}^{0.5} \quad (2)$$

where E_{Si} is the electron kinetic energy (37 eV for Si 2p photoelectrons under our measurement conditions). By using this method, the escape depth of photoelectrons in the Si 2p peak was calculated to be λ_{Si} = 3.5 Å. Electron escape depths in Si measured previously under similar conditions have been reported to be 3.2−3.6 Å.[9,10]

To identify features in the Si 2p region in addition to the bulk Si 2p peak, the background was determined with use of a Shirley fitting procedure[11−13] and subtracted from the original spectrum. The background-subtracted spectra were then processed to deconvolute, or "strip", the Si $2p_{1/2}$ peak from the spin−orbit doublet.[10,14] To perform the spin−orbit stripping procedure, the energy difference between the Si $2p_{3/2}$ and Si $2p_{1/2}$ peaks was fixed at 0.6 eV, and the Si $2p_{1/2}$ to Si $2p_{3/2}$ peak area ratio was fixed at 0.51.[4,10,14,15] The residual spectrum composed of Si $2p_{3/2}$ peaks was then fit with a series of Voigt line shapes[16] that were 5% Lorentzian and 95% Gaussian functions.[5,15] Once optimal fitting parameters for Si^{+}−Si^{4+}

surfaces were determined for the fully oxidized Cl-terminated surface, those parameters were used to fit all other surfaces, to determine any differences between samples in the distribution of specific oxidation states of Si.

A simple overlayer-substrate model was employed to calculate the total monolayer coverage of surface species observed by SXPS.[5,14,15] In this method, the number density of modified surface Si atoms, $\Gamma_{Si,surf}$, was deduced from the ratio of the integrated area under the Si peak assigned to the surface atoms, $I_{Si,surf}$, to the integrated area of the Si peak assigned to bulk Si atoms, $I_{Si,bulk}$, with

$$\frac{I_{Si,surf}}{I_{Si,bulk}} = \frac{\Gamma_{Si,surf}\sigma_{Si,surf}}{n_{Si,bulk}\sigma_{Si,bulk}l_{Si} - \Gamma_{Si,surf}\sigma_{Si,surf}} \quad (3)$$

In this expression, $n_{Si,bulk}$ is the atom density of bulk crystalline Si (5.0×10^{22} cm^{-3}),[8] $\sigma_{Si,surf}$ and $\sigma_{Si,bulk}$ are the photoionization cross-sections of the surface and bulk species, respectively, and l_{Si} is the electron escape depth, calculated from $l_{Si} = \lambda_{Si} \sin \theta$, where θ is the collection angle measured off the surface. The data presented herein were collected at $\theta = 90°$, so $l_{Si} = 3.5$ Å. The photoionization cross-sections of Si^0-Si^{4+} species have been studied extensively by SXPS on surfaces with well-ordered SiO_2 layers of known thicknesses.[14] Near the photon excitation energy used in this work (140 eV), $\sigma_{SiO_2}/\sigma_{Si} \sim 2$, while $\Gamma_{SiO_2}/n_{Si} \sim 0.5$, thus approximately canceling out of the surface intensity factor.[14] For the highly amorphous suboxides grown in air in these studies, $n_{Si^{n+}}$ values are not known, cannot be accurately estimated, and would have to be measured from studies of the thickness of the disordered layer. Therefore throughout the analysis, $\sigma_{Si^{n+}}$ was approximated as constant for Si^+-Si^{4+}, simplifying eq 3 to:

$$\frac{I_{Si,surf}}{I_{Si,bulk}} = \frac{\Gamma_{Si,surf}}{n_{Si,bulk}l_{Si} - \Gamma_{Si,surf}} \quad (4)$$

Substituting $I = I_{Si,surf}/I_{Si,bulk}$ and $\Gamma_{Si,bulk} = n_{Si,bulk}l_{Si}$ into eq 4 and rearranging yields

$$\Gamma_{Si,surf} = \frac{I}{1+I}\Gamma_{Si,bulk} \quad (5)$$

Dividing the calculated value of $\Gamma_{Si,surf}$ by the number density of atop sites on the Si(111) surface, $n_{Si,surf} = 7.8 \times 10^{14}$ cm^{-2},[14] gives the monolayer coverage of modified Si atoms. The distance between Si layers along a vector perpendicular to the Si(111) crystal face is 1.6 Å,[17] implying that an electron escape depth of 3.5 Å will sample 2.2 monolayers of the Si crystal.

2. XPS Measurements. To determine the influence of step edges on the oxidation of functionalized Si(111) surfaces, core photoelectron spectra were collected with an M-Probe XPS system that has been described previously.[4,5] For these experiments, 1486.6 eV X-rays generated from an Al Kα source illuminated the sample from an incident angle of 35° off the surface. Photoelectrons emitted along a trajectory 35° off of the surface plane were collected by a hemispherical analyzer. Samples were inserted via a quick-entry load lock into the UHV system and were kept at a base pressure of $\leq 1 \times 10^{-9}$ Torr. All samples were sufficiently electrically conductive at room temperature that no compensation for charging effects was required. Deconvolution of the silicon oxide region was conducted as described above. To calculate the monolayer coverage of the oxide peak, a slightly different procedure was followed because of the higher escape depth of photoelectrons with this technique (16 Å).[5] The monolayer coverage was calculated directly from the SiO_x:Si 2p peak area ratio by comparing that ratio to the value that would be expected for a Si surface on which 100% of Si atoms had oxidized.[5] Substituting into eq 4 yields a value of $I_{Si,surf}/I_{Si,bulk} = 0.21$ for a Si(111) surface on which 100% of Si atoms have oxidized. The observed SiO_x:Si 2p area ratio was therefore divided by this normalization constant to determine the monolayer coverage of that suboxide species.

3. SAM Measurements. Spatial resolution of surface oxidation was obtained on a Physical Electronics (Phi) 680 Scanning Auger Nanoprobe at the High-Temperature Materials Laboratory at Oak Ridge National Laboratory. The sample was introduced through a load lock into a UHV chamber maintained at $\leq 10^{-10}$ Torr. The sample was impinged with an electron beam that was held normal to the surface and maintained at 20 kV and 10 nA, for a spatial resolution of 15 nm. Auger electrons were collected by a cylindrical mirror analyzer coaxial to the field emission electron gun. Secondary electron images of the sample were used to identify a debris-free region of the sample surface. Auger electron intensities were then collected over an area approximately 1 μm square divided into 128 × 128 bins, producing a pixel width of 7.8 nm. The scan area was periodically calibrated with a scanning electron microscope (SEM) image of a nearby dust particle to account for spatial drift in the image over the scan time. Between 1 and 5 such scans were added together for the final image. Data were collected quickly to minimize damage to the alkyl overlayer by the impinging electron beam. Because the amount of SiO_2 on the surface of alkylated samples was very small, it was not possible to collect spectra of the SiO_2 signal (72−76 eV) in a short enough amount of time to prevent beam damage. Instead, signals from the Si LVV (90−92 eV)[18−20] and O KLL (510 eV)[21] regions were combined to determine areas of SiO_2 in the SAM image. Spectra were collected with the electron analyzer held in the Si LVV region (92 eV) and the O KLL region (510 eV), which were then superimposed to create a composite image of Si and SiO_2.

III. Results

A. SXPS Analysis of Functionalized Surfaces. *1. Cl-Terminated Si(111) Surfaces*. Figure 1a shows the SXPS data on a Cl-terminated Si(111) surface immediately after preparation. The spectrum is displayed after subtraction of the Shirley background and after spin−orbit stripping, leaving only the $2p_{3/2}$ component of the Si peak. The freshly prepared surface, which has been described previously,[22] displayed a peak 0.83 eV higher in binding energy than the bulk Si $2p_{3/2}$ peak, which represented a surface coverage of 0.99 equivalent monolayers (ML). This peak has been assigned to the chlorinated surface Si atoms, which are more electropositive than the Si atoms in the bulk lattice because of the electron-withdrawing effects of Cl. A small feature 1.37 eV higher in binding energy than the bulk peak, which represented 0.11 equivalent ML, has been tentatively assigned to dichlorinated Si presumably present along step edges or etch pits.

A survey XPS scan of the freshly prepared surface, shown in Figure 2a, revealed Si, Cl, C, and some oxygen, as evidenced by the O 1s signal at 540 binding eV (along with the characteristic spike in noise after a strong signal, observable in this spectrum at 550 eV) and by the O $K_1L_{23}L_{23}$ Auger peak at ≈970 binding eV. Using the known escape depth of Si 2p photoelectrons and correcting for the different cross sections of the O 1s and Si 2p signals, the ratio of the O 1s intensity to the Si 2p intensity corresponded to ≈1.4 monolayer equivalents of O. However, this oxygen signal is not associated with

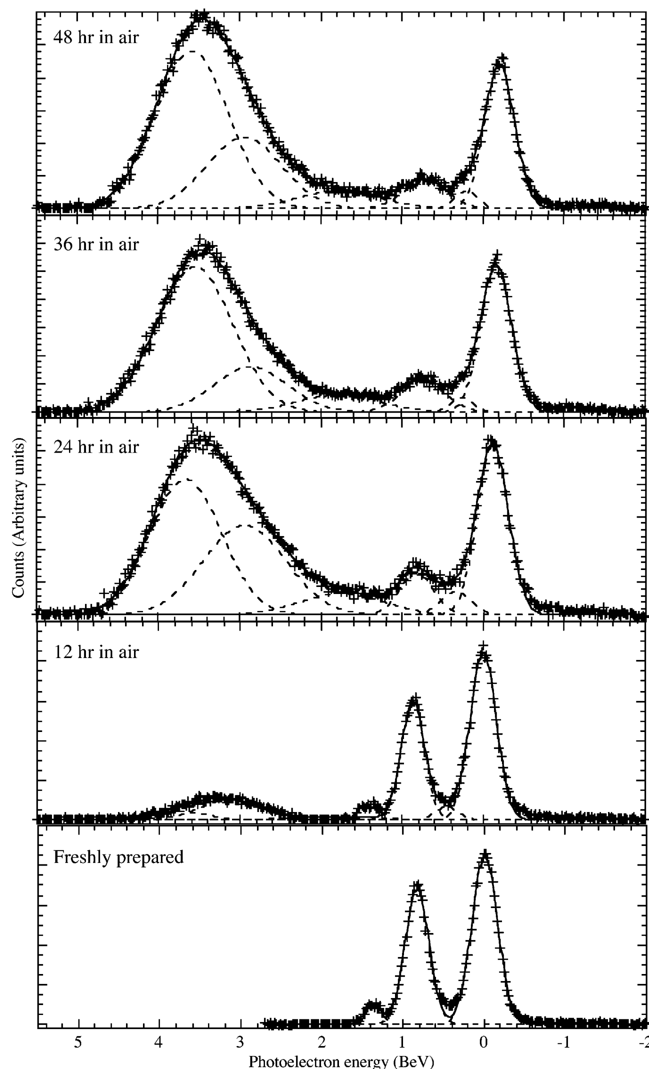

Figure 1. Soft X-ray photoelectron spectra of a chlorine-terminated Si(111) surface as a function of exposure to air. The abscissa displays the binding energy (BeV) relative to the center of the bulk Si $2p_{3/2}$ peak of the freshly prepared surface. All spectra are shown after background removal, spin−orbit stripping, and peak fitting. The cross marks are the raw data, the dashed lines are the fitted curves, and the solid lines are the calculated curve fits. The anomalous break in the pattern of growth of Si suboxides on the sample kept in air for 24 h was most likely due to some contribution to the signal from the sample holder because of an ill-focused beam.

oxidation of the surface or near-surface Si, because negligible (below 0.1 monolayer) levels of oxidized Si are observed for such surfaces in the high binding energy area of the Si 2p region, even by highly surface sensitive SXPS (Figure 1).[22] Consistently, <15% of a monolayer of silicon oxide is observable by transmission infrared spectroscopy on the freshly prepared Cl-terminated Si(111) surface.[23] The O 1s XPS signal could arise from a number of sources, including adsorbed solvent from the wet chemical preparation techniques, adsorbed pump oil vapor introduced in the quick-entry load lock, or contaminating dust particles covered with oxygen-containing organic molecules that were not possible to avoid when working in standard laboratory conditions.

The principal concern of this study was the subsequent growth and characterization of silicon oxides, and because of the uncertainty of the origin of the O 1s signal, this peak was not used to identify the presence of silicon oxides on the surfaces described here. The Si 2p region, which has specific and extensively studied spectroscopic shifts introduced by Si^{+}−Si^{4+}

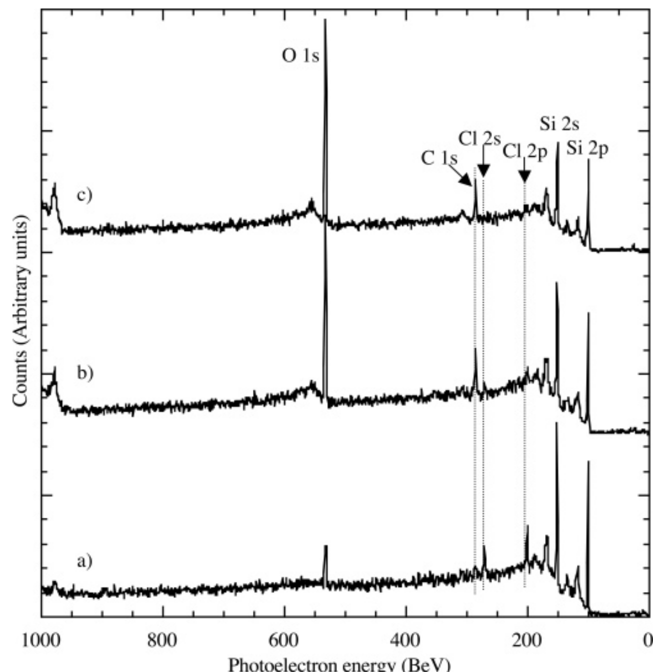

Figure 2. Survey scan XPS data on Cl−Si(111) surfaces as a function of time exposed to air: (a) freshly prepared surface; (b) after 20 h in air; and (c) after 54 h in air.

oxides,[10,14] was examined to address this question. The presence of a strong signal from Si−Cl at +0.83 eV higher in energy than the Si $2p_{3/2}$ bulk peak could obscure the presence of any mono-oxidized Si^{+}, which would be expected at ≈+0.9 eV.

When exposed to ambient air (Figure 1b−e), the chlorinated Si surface reacted rapidly, showing a decrease in the intensity of the Si−Cl and $Si-Cl_2$ features and an increase in peaks at higher binding energy ascribable to silicon oxides. After 12 h in air (Figure 1b), the monolayer coverage of the peak approximately 0.8 eV higher in binding energy than the bulk peak, assigned to surface Si bonded to Cl atoms, dropped from 0.99 ML[22] to 0.87 ML, the 1.37 eV signal also decreased in intensity, and a broad signal of oxide, centered at +3.13 eV above the bulk Si $2p_{3/2}$ peak, appeared. This oxide feature was accompanied by smaller suboxides 1.85 and 3.74 eV, respectively, above the bulk Si $2p_{3/2}$ peak. The oxide signals collectively represented a total equivalent coverage of 1 ML of silicon oxides. The broad peak attributed to a silicon suboxide centered at +1.85 eV above the bulk Si $2p_{3/2}$ peak obscured any small residual signal at +1.37 eV ascribed on the freshly prepared surface to dichlorinated Si. The results of a peak-fitting decomposition of the observed SXPS signals into Si oxides of various oxidation states, along with the equivalent monolayer coverage of each surface species, are presented in Table 1.

As air exposure of the Cl−Si(111) surface continued, the growth of the surface oxide features correlated qualitatively with a decrease in the signal at 0.9 eV above the bulk Si $2p_{3/2}$ peak arising from surface Cl-bound Si atoms. As can be seen in Table 1 and Figure 1, after the surface had been exposed to air for 12 h, the monolayer coverage of the highest order Si oxide (Si^{4+}, +3.74 eV) grew from below the detection limit of the instrument to 0.21 ML. After 24 h of exposure to air, the Cl-bound Si signal had decreased to ∼0.5 ML, while the highest order oxide (Si^{4+}, +3.78 eV) signal increased to an equivalent coverage of 1.45 ML. An XPS survey scan of the Cl-terminated surface collected after the sample had been exposed to air for 20 h (Figure 2(b)) confirmed that the intensity of the Cl 2p and 2s signals at 200 BeV and 270 BeV, respectively, had decreased significantly

TABLE 1: Si $2p_{3/2}$ SXPS Data on Functionalized Si Surfaces Oxidized in Air for up to 48 hr

					silicon oxides								
			surface Si−X		"Si^{+}"		"Si^{2+}"		"Si^{3+}"		"Si^{4+}"		
R−Si(111) R−	time in air (h)	bulk peak[a] binding energy (eV)	shift (eV)	coverage (ML)	shift (eV)	coverage (ML)	shift (eV)	coverage (ML)	shift (eV)	coverage (ML)	shift (eV)	coverage (ML)	total surface coverage (ML)
						X = Cl							
Cl−	12	98.64	0.87	0.87	*b*	*b*	1.85	0.15	3.13	0.49	3.74	0.21	1.87
	24	98.52	0.94	0.47	*b*	*b*	1.86	0.57	3.06	1.30	3.78	1.45	4.06
	36	98.48	0.89	0.53	*b*	*b*	1.94	0.53	3.02	0.95	3.71	1.59	3.75
	48	98.44	0.92	0.49	*b*	*b*	1.99	0.57	3.15	1.24	3.79	1.62	4.12
						X = C							
CH_3−	12	98.04	0.30	1.03	0.79	0.08							1.11
	24	98.04	0.31	0.86	0.76	0.06	1.76	<0.01	3.11	0.05	3.88	0.04	1.02
	36	98.08	0.30	0.95	0.79	0.08	1.72	<0.01	3.07	0.05	3.75	0.09	1.17
	48	98.05	0.31	0.89	0.75	0.07	1.75	<0.01	3.10	0.13	3.80	0.07	1.16
C_2H_5−	12	98.19	0.19	0.77	0.61	0.23	1.57	0.04					1.04
	24	98.21	0.17	0.66	0.74	0.23	1.78	0.07	3.12	0.06	3.87	0.03	1.05
	36	98.19	0.21	0.76	0.81	0.17	1.85	0.07	3.10	0.13	3.84	0.02	1.15
	48	98.19	0.21	0.71	0.81	0.24	1.85	0.14	3.10	0.15	3.84	0.09	1.33
$C_6H_5CH_2$−	12	98.24	0.18	0.56	0.79	0.33	1.79	0.06	3.16	0.10	3.81	0.03	1.07
	24	98.25	0.17	1.00	0.78	0.27	1.78	0.04	3.19	0.08	3.75	0.03	1.43

[a] Absolute energies for the bulk Si $2p_{3/2}$ peak are reported for thoroughness, but are of limited use because the excitation energy was not calibrated. [b] No deconvolution of the shifts of Si−Cl and Si^{+} was attempted.

from those observed on the freshly prepared surface, indicating that most of the Cl present on the surface had disappeared. At this point it was difficult to determine if the SXPS peak previously assigned as Cl-bound surface Si atoms was actually cleanly functionalized Cl−Si or rather represented an amorphous Si^{+} substrate. Furthermore, the survey XPS revealed a dramatic increase in O 1s and O $K_1L_{23}L_{23}$ Auger signals at 540 and 970 BeV, respectively, as well as a more pronounced appearance of the characteristic spike in background noise immediately after the O 1s signal (feature seen at ∼550 BeV).

After the Cl−Si surface had been exposed to air for ≈48 h, the XPS survey scan indicated only a small amount of Cl remained on the surface (Figure 2c). Again, features associated with large amounts of O on the surface dominated the spectrum at 540 and 970 binding eV. The apparent shift in the Si $2p_{3/2}$ binding energy seen in Figure 1 could be explained by a slight shift in the energy of the excitation beam over the course of the experiment (10 days). Because this experiment was concerned with the relative position of silicon oxides at higher energy than the Si $2p_{3/2}$ bulk peak, all data in Figure 1 are shown relative to the position of the Si $2p_{3/2}$ bulk peak on the freshly prepared Cl−Si(111) surface. A small feature at 0.5 eV, of unknown origin but possibly due to Si−OH or absorbed water on the surface, was apparent. More prominent features, representing Si^{2+} (+1.99 eV), Si^{3+} (+3.15 eV), and Si^{4+} (+3.79 eV) oxides, dominated the spectrum in the Si 2p region (Figure 1e), with the Si^{4+} oxide peak having an apparent surface coverage of 3.63 ML. Because a penetration depth of 3.5 Å used in these studies only sampled approximately 2.2 ML perpendicular to the (111) crystal face, this high monolayer coverage is possibly a result of the limitations of the quantitative analysis of surface species described by eq 5, which does not account for differences in σ or n of the substrate or overlayer, and which might therefore be inadequate for the amorphous surface described here. After 48 h in air, however, the Cl-terminated Si(111) surface had thoroughly reacted with ambient air to create an amorphous silicon oxide layer that, on the scale of our surface sensitive conditions, was reasonably thick. These results were nominally identical for the H-terminated Si(111) surface that was allowed to oxidize in air for 48 h, although the freshly etched surface was partly compromised by a Si^{+} oxide, and so is not described here in any further detail.

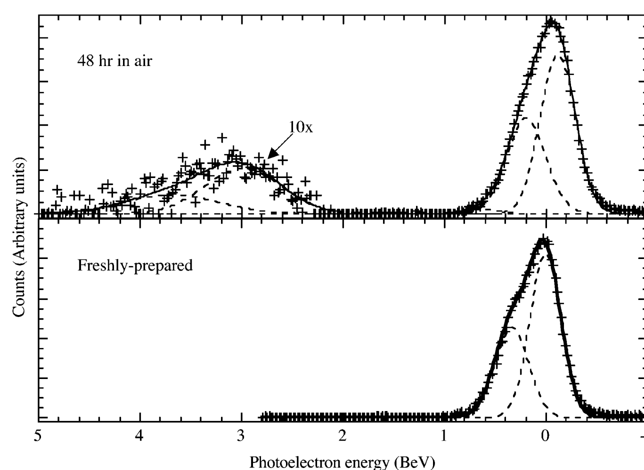

Figure 3. SXPS spectra of a CH_3-terminated Si(111) surface as a function of time in air. The abscissa is binding energy (BeV) relative to the center of the Si $2p_{3/2}$ bulk peak of the freshly prepared surface. All spectra are shown after background removal, spin−orbit stripping, and peak fitting. The cross marks are the raw data, the dashed lines are the fitted curves, and the solid lines are the calculated curve fits. In the spectrum of the oxidized surface (b), the region above 2 eV is shown expanded 10× in signal intensity.

2. CH_3-Terminated Si(111) Surfaces. Figure 3 presents SXPS data for a CH_3-terminated Si(111) surface being oxidized by air. Like the Cl-terminated Si(111) surface described previously, a slight shift in the binding energy of the Si $2p_{3/2}$ bulk peak was observed over the course of the experiment. Because this could have been caused by a shift in the energy of the excitation beam, all data are shown referenced to the binding energy of the Si $2p_{3/2}$ bulk peak on the freshly prepared surface.

In contrast to the Cl-terminated surface, relatively little spectral changes in the silicon oxide region were observed for the CH_3-terminated Si surface upon exposure to an air ambient. The extremely small growth of silicon oxides on this sample made deconvolution difficult, so peaks were fitted by using the values of the centers of the Si^{+}−Si^{4+} peaks on the oxidized Cl-terminated surface. After 48 h in air, the peak at 0.3 eV higher binding energy than the bulk Si $2p_{3/2}$ peak, assigned to

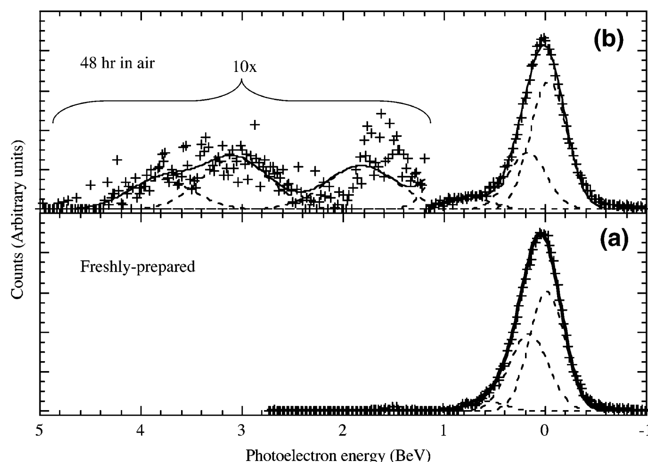

Figure 4. SXPS data of a C_2H_5-terminated Si(111) surface as a function of time in air. The signal processing and the meaning of the abscissa and data labels are the same as in Figure 3. In the spectrum of the oxidized surface (b), the region above 1 eV is shown expanded 10× in signal intensity.

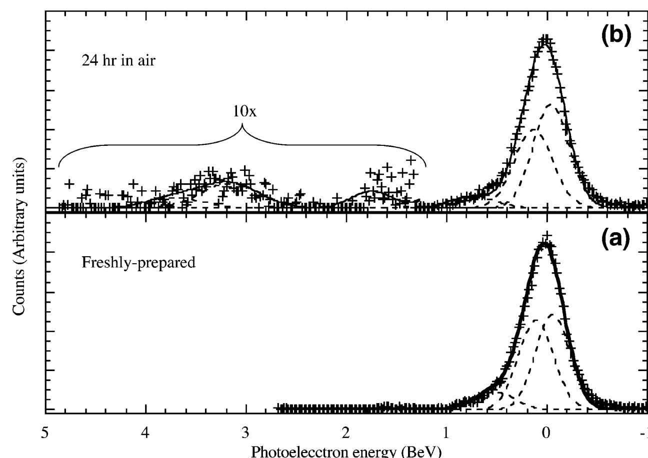

Figure 5. SXPS data of a $C_6H_5CH_2$-terminated Si(111) surface as a function of time in air. The signal processing and the meaning of the abscissa and data labels are the same as in Figure 3. In the spectrum of the oxidized surface (b), the region above 1 eV is shown expanded 10× in signal intensity.

surface Si atoms bonded to the methyl carbon atom,[22] did not shift substantially in binding energy or intensity. A broad feature, centered on the Si^{3+} oxidation state at +3.10 eV above the bulk Si $2p_{3/2}$ peak, was evident and had an equivalent coverage of 0.20 ML. No Si^{2+} was observed, and signals for Si^{+}, Si^{3+}, and Si^{4+} species were observed in quantities just above the detection limit of the instrument. No further increase in suboxide coverage, no peak shifts, nor any other substantial change on the surface was observed when these samples were reexamined after 2 months of exposure to ambient air.

3. C_2H_5-Terminated Si(111) Surfaces. The rate of air oxidation of C_2H_5-terminated Si surfaces (Figure 4, Table 1) as monitored by SXPS was similar to that of CH_3-terminated Si surfaces. A feature in the spectrum of the freshly prepared ethyl-terminated surface at 0.19 eV above the bulk Si $2p_{3/2}$ peak, previously identified as in part due to surface Si atoms bonded to the C of the ethyl group,[22] did not shift significantly over time, indicating that the Si−C bonds formed in the alkylation procedure were not substantially altered by exposing the surface to ambient air. A peak observed on the freshly prepared surface 0.81 eV higher in binding energy than the silicon bulk peak also did not increase in amplitude with time, comprising 0.25 ML after 48 h of air exposure. At 48 h of air exposure, small features corresponding to silicon oxides were observed at ca. +1.85, +3.10, and +3.84 eV higher in binding energy than the bulk Si $2p_{3/2}$ peak. For consistency, the peaks were fitted by using center positions of the different Si oxidation states that were observed on the oxidized Cl−Si(111) surface. These signals together comprised 0.62 equivalent ML of oxide, with the Si^{+} species representing the greatest portion of detectable suboxide.

4. $C_6H_5CH_2$-Terminated Si(111) Surfaces. The SXPS data on the air oxidation of $C_6H_5CH_2$-terminated Si(111) surfaces is displayed in Figure 5 and Table 1. After 1 day in air, peaks present on the freshly prepared surface, at ∼0.2 and ∼0.8 eV higher binding energy than the bulk Si $2p_{3/2}$ peak, changed binding energy and intensity only slightly. During this time period, small oxide peaks at 1.78, 3.19, and 3.75 eV higher than the bulk Si $2p_{3/2}$ peak, together representing <0.5 ML, were observed. As on the C_2H_5-terminated Si(111) surface, the Si^{+} and Si^{3+} peaks (+0.78 and +3.19 eV above the Si $2p_{3/2}$ bulk peak, respectively) comprised the majority of the oxide signal.

B. Oxidation Rates of Stepped Samples. To determine if the Si surface alkylation process inhibited oxidation by inhibiting step edge-mediated oxidation processes,[24] alkyl-terminated surfaces of differing step edge density were prepared and stored in ambient air in the dark for a period of up to 6 weeks. On a surface with a 0.5° miscut, approximately 1 in every 600 surface Si atoms is along a step edge, whereas 1 in every 7 surface Si atoms is along a step edge on a surface with a 7° miscut angle off of the (111) orientation. After normalization for peak intensity, essentially no difference was observed in the native oxide growth upon air exposure for these two different miscut angle surfaces (Figure 6). When the spectra were deconvoluted into the characteristic oxidation peaks of Si, contributions from Si^{+} and Si^{3+} species were again a larger part of the Si oxidation peak than the other two available oxidation states (Table 2).

C. SAM Data on Alkyl-Terminated Si(111) Samples. Scanning Auger microscopy was used to evaluate the spatial homogeniety of the oxidation of alklylated Si surfaces. Spatially resolved spectral maps were collected on each surface of interest in the Si LVV region at 92 eV and in the O KLL region at 510 eV. For each surface, the two spectral maps were then superimposed to create a composite image of the elemental distribution on the surface.

On a freshly prepared C_2H_5−Si(111) sample, the composite SAM image maps revealed a homogeneous surface (Figure 7). SAM maps, however, revealed discrete, chemically altered regions of the surface on an identically prepared C_2H_5−Si(111) sample that had first been exposed to air and light for 8 days. A regular SEM image (Figure 8a) of this oxidized surface exhibited discolored portions of the Si surface which appeared in patches running approximately parallel to each other. The lightly colored patches showed a decreased concentration of Si^{0} but an increased concentration of O when compared to the otherwise clean Si background (Figure 8b). In the SAM image of the same area, these patches appeared as areas deficient in the Si LVV signal at 92 eV and had higher concentrations of O in the O KLL energy region (Figure 8a).

IV. Discussion

Alkylation of Si(111) with the two-step chlorination/alkylation process results in a remarkable degree of chemical and electronic passivation of the Si surface.[1,5] The chemical passivation is manifest as a very large suppression in the rate of oxide formation, with only a fraction of an equivalent monolayer formed after months in ambient air, as opposed to after minutes

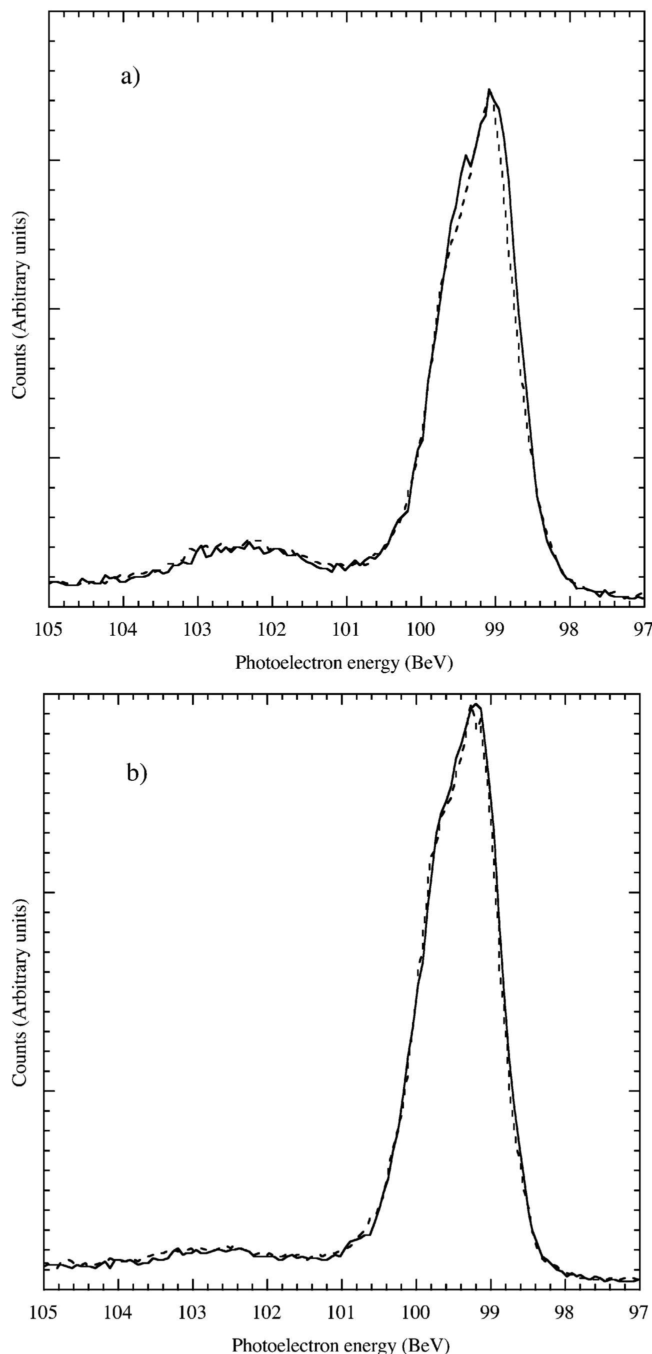

Figure 6. XPS data in the Si 2p region of alkyl-terminated Si(111) surfaces having different miscut angles. The spectra have been normalized for intensity. (a) CH_3−Si(111) samples that had been stored in ambient air in the dark for 39 days: (solid line) surface miscut ≤0.5°; (dashed line) surface miscut 7°. (b) C_2H_5−Si(111) samples that had been stored in ambient air in the dark for 19 days: (solid line) surface miscut ≤0.5°; (dashed line) surface miscut 7°.

for a Cl-terminated or H-terminated Si(111) surface.[1,5] The electrical passivation is manifest as a remarkably low number of electrically active defects sites on the alkylated surfaces, as measured by an extremely low surface recombination velocity, *S*, for extended time periods in an air ambient.[1] The present SXPS studies aid in elucidation of three key mechanistic issues regarding the alkyl passivation process. One question concerns why the surface recombination velocity is small even when alkyl groups are used that cannot sterically terminate every atop site on an unreconstructed Si(111) surface. A second question concerns how the surface recombination velocity remains low even after oxide is detectable spectroscopically on alkylated surfaces exposed for extended periods of time to ambient air. A third question concerns factors that influence how sterically large alkyls suppress the rate of oxidation on functionalized Si surfaces, despite being too large to terminate every Si atop site.

A. Initial Electrical Passivation Properties of Alkylated Si(111) Surfaces. The electrical passivation of freshly alkylated Si surfaces is relatively straightforward to understand.[1,5] Methyl groups can, in principle, terminate every Si atop site on an unreconstructed (1 × 1) Si(111) surface. Recent STM work has revealed such an extended (1 × 1) surface structure for CH_3-terminated Si surfaces prepared by using the two-step chlorination/alkylation procedure.[25] This high surface coverage, along with the expectation that methyl groups form strong, kinetically inert Si−C bonds to the atop Si atoms on (111)-oriented Si surfaces, is consistent with the observed lack of electrical trap sites due to dangling or weak chemical bonds on methyl-terminated Si(111) surfaces.[1,5]

The electrical passivation on surfaces alkylated with saturated alkyls other than methyl can also be understood. Although non-methyl saturated alkyl groups cannot sterically cover every atop site on the Si surface, due to van der Waals interactions between methylene groups on adjacent alkyls, freshly prepared alkylated Si surfaces showed no detectable oxide (i.e., <10% of a monolayer) even with the surface-sensitive SXPS methodology. Infrared spectroscopy has shown that the spectroscopically active Si sites on such surfaces that are not terminated with Si−C bonds are terminated with Si−H bonds,[26] consistent with the small but observable chemical shift of the surface Si atoms in the SXPS data reported herein (Figures 3−5) and reported previously.[22] Because H−Si(111) and CH_3−Si(111) surfaces both show very low surface recombination velocities, it is reasonable that a mixed Si−H/Si−C terminated surface would also exhibit a low surface recombination velocity. On alkylated Si(111) surfaces, the Si atop sites participate in four relatively strong chemical bonds (three Si−Si bonds and a fourth Si−H or Si−C bond), fully terminating their tetrahedral geometry and sp^3-hybrid bonding requirements, as is the case for atoms in the bulk of the Si.

B. Surface Recombination Velocity of Oxidized, Cl-Terminated Si Surfaces vs Oxidized, Alkyl-Terminated Si Surfaces. The SXPS data (Figure 1) clearly indicate that the Cl-terminated Si(111) surface oxidizes rapidly. During this process, a significant amount of oxide is formed, the Si−Cl bonds are cleaved, and the oxidation states of the resulting oxide span from Si(I) to Si(IV). This behavior is consistent with insertion of oxygen into Si−Si back-bonds, along with a reaction between the Si−Cl bonds on atop sites with water in the air, to form SiO_2 and to allow facile propagation of oxide growth on the resulting Si surface. Such air-exposed surfaces are not only readily and significantly oxidized, but also have a high electrical surface recombination velocity. In contrast, on alkylated Si surfaces, Si(IV) is not observed, and the small amount of oxide that does eventually form is predominantly Si(III) in character (Figure 5). Because the Si oxide formed on alkylated Si surfaces does not apparently produce an electrically defective surface, alkylated Si surfaces retain their remarkable electrical properties over extended time periods in an air ambient and are in fact tolerant of small amounts of oxide growth on the surface.

C. Chemical Considerations for the Oxidation of Alkylated Si Surfaces. For the alkylated Si surfaces, the oxidation reactions are so slow (days to months) that the oxidation reagent is not known definitively. Either the observed reaction rate reflects the inherent oxidation rate of such surfaces with oxygen

TABLE 2: Si $2p_{3/2}$ XPS Data on Functionalized Si Surfaces of Varying Step Size Oxidized in Air for up to 40 days

			silicon oxides								
			"Si^{+}"		"Si^{2+}"		"Si^{3+}"		"Si^{4+}"		
R−Si(111) R−	miscut angle (deg)	bulk peak[a] binding energy (eV)	shift (eV)	coverage (ML)	shift (eV)	coverage (ML)	shift (eV)	coverage (ML)	shift (eV)	coverage (ML)	total surface coverage (ML)
CH_3−	0.5	98.91	0.99	0.56	2.0	0.12	3.09	0.41	4.04	0.09	1.19
	7	98.89	1.01	0.48	2.01	0.12	3.08	0.45	3.91	0.15	1.21
C_2H_5−	0.5	99.11	0.89	0.68	1.97	0.09	3.17	0.11	3.99	0.05	0.93
	7	99.13	0.87	0.72	2.0	0.08	3.16	0.17	3.97	0.05	1.01

[a] Absolute energies for the bulk Si $2p_{3/2}$ peak are reported for thoroughness, but are of limited use because the excitation energy was not calibrated.

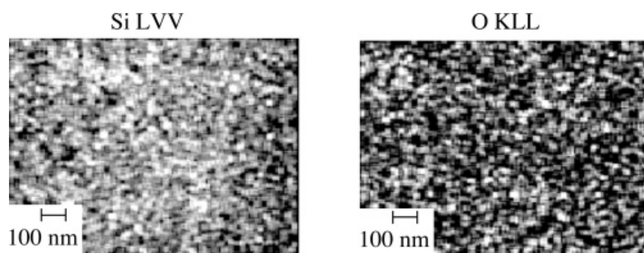

Figure 7. SAM image of a freshly prepared C_2H_5-terminated Si(111) surface investigated in both the Si LVV region (92 eV, left) and the O KLL energy regions (510 eV, right). Both images were collected in 128 × 128 point scans with an electron beam held at 20 kV and 10 nA with a spatial resolution of 15 nm. The individual pixel scans were combined to form an image map.

and/or water that are present in air, or it reflects a reaction controlled predominantly by trace impurities (ozone etc.) present at low levels in the air to which the samples were exposed. Regardless of the exact mechanism of oxidation under the conditions investigated, it is clear that alkylation dramatically inhibits the oxidation of such samples, producing stability for months/days in the presence of oxygen, water, and trace impurities in the ambient air environment.

A key observation with regard to assessing the air oxidation of alkylated Si is that although H_3C-terminated Si(111) surfaces oxidized extremely slowly and to a limited extent, the primary oxidation product detectable by SXPS was Si(III), along with some lower oxidation state Si oxides. Additionally, unlike the situation for the Cl-terminated Si(111) surface, which loses surface Si−Cl bonds concomitant with oxidation, the SXPS data indicate that on alkylated surfaces, the Si−C bonds remain on the surface even when some of the Si atoms become oxidized. A second key observation is that H_5C_2- and benzyl-terminated Si(111) surfaces exhibit very similar behavior to CH_3−Si(111) both in terms of their rate of oxidation and the distribution of oxidation state of the resulting Si surface species (Figures 4 and 5). A third key observation is that the SAM data indicate that the oxide that does form on alkylated Si surfaces grows spatially inhomogeneously, being dominated by aligned striations on the surface (Figure 8). A fourth key observation is that the rate and spatial distribution of oxide growth are not affected by a significant increase in the step edge density, as evidenced by similar behavior on Si(111) surfaces relative to vicinal, miscut surface orientations with a high degree of step edges (Figure 6).

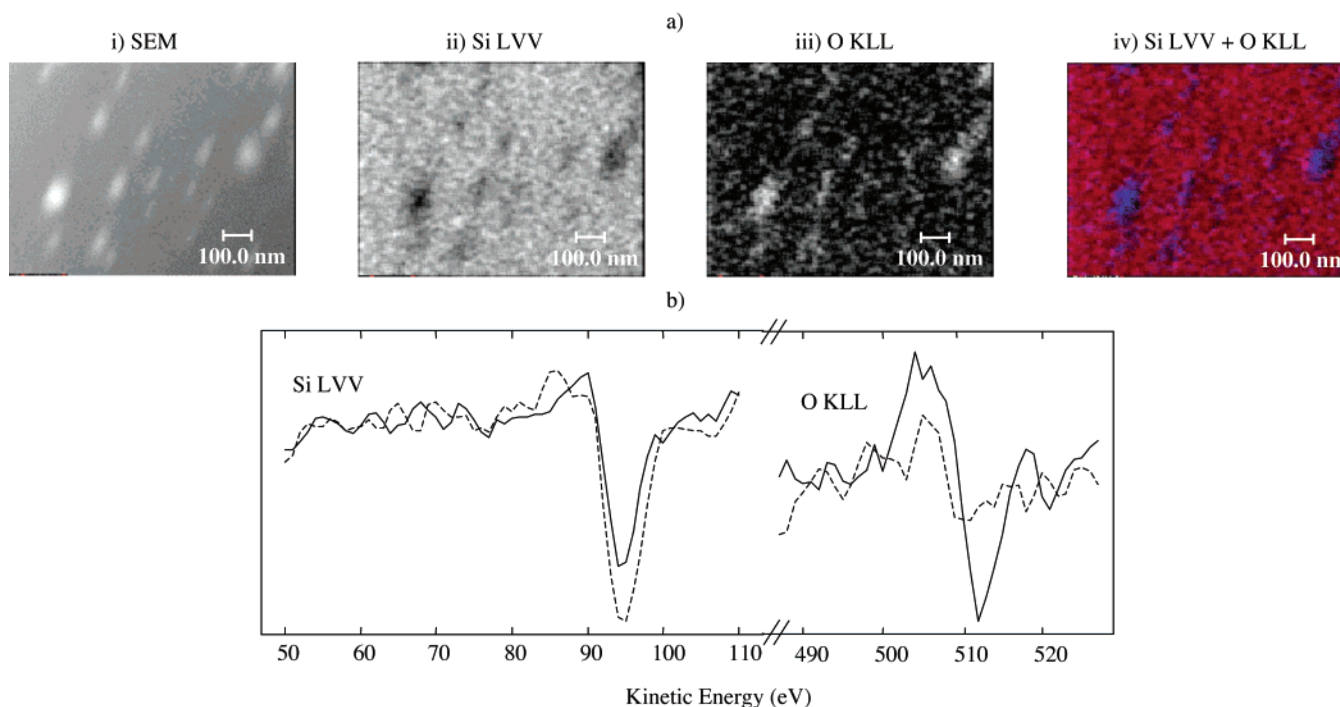

Figure 8. Auger electron spectroscopy of a C_2H_5-terminated Si(111) surface exposed to air for 8 days. (a) SAM images of a ~1 μm^2 area of the surface: (i) SEM image of the surface; (ii) SAM image collected by scanning in the Si LVV energy region (92 eV) (lighter gray indicates a greater Si signal); (iii) SAM image collected by scanning in the O KLL energy region (510 eV) (lighter gray indicates a greater O signal); (iv) composite SAM image of the overlayed maps of the Si LVV (red) and O KLL (blue) energy regions. SAM images were collected in 128 × 128 point scans with an electron beam held at 20 kV and 10 nA with a spatial resolution of 15 nm. The individual pixels were then combined to form an image map. (b) AES spectra of a point on an isolated white discolored region in the SEM image (solid line) and of a point on the dark background in the SEM image (dashed line).

SCHEME 1

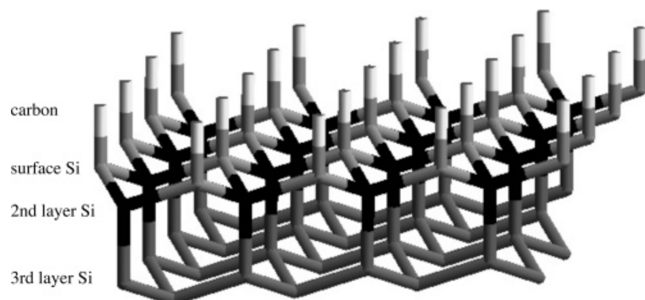

The extremely slow observed rate of oxidation in an air ambient indicates that both Si−C bonds and Si−H bonds located adjacent to Si−C bonds on the terraces of alkylated Si surfaces are relatively inert kinetically. The slow oxidation rate further indicates that either all of the investigated alkyls passivate the step edges or that step edges or kink sites are not the active sites for observable oxidation on such surfaces relative to defects on terraces. Clearly the data with bulky alkyl groups indicate that even a relatively sparse population of Si−C bonds is sufficient to inhibit oxide growth from propagating both laterally and vertically relative to the surface plane, precluding formation of the deleterious type and amount of Si oxide that produces a high surface recombination velocity during the air ambient oxidation of either the Cl- or H-terminated Si(111) surfaces.

On the H-terminated Si(111) surface, oxidation requires the presence of both an oxidant, O_2(g), and a nucleophile, H_2O.[27,28] Furthermore, the mechanism of oxidation on Si−H surfaces has been proposed to involve insertion of O into the Si−Si back-bonds.[29−31] Previous core photoelectron spectroscopic studies of the Si(111)/SiO_2 interface have shown that Si(I) and Si(III) are more abundant than Si^{2+} because disrupting an atomically flat (111) surface through layer-by-layer oxidation will cleave either 1 or 3 Si tetrahedral bonds.[6,14,32−35] Two Si bonds will be cleaved only at step edges and etch defects, which are a minor component of Si(111) surfaces prepared in this manner. Additionally, the native oxide that forms on an unpassivated H- or Cl-terminated Si(111) surface covers all available oxidation states of Si, from Si(I) to Si(IV), with the majority of the oxide signal appearing as Si(IV) species.[34,36−38]

One possible way to understand this set of observations involves the representation of the Si(111) surface shown in Scheme 1, in which the surface-bound carbon atoms are shaded white, the first layer silicon atoms are shaded light gray, the second layer silicon atoms are shaded black, and the rest of the bulk silicon crystal is shaded dark gray. First, the second layer Si atoms (Scheme 1, black atoms) could possibly have the three Si−Si bonds to the first layer oxidized Si atoms (Scheme 1, light gray atoms). However, the oxidation process halts at this point, preventing insertion of an oxygen atom into the Si−Si bond leading to the third layer oxidized Si atoms (Scheme 1, dark gray atoms). This would leave second layer Si atoms in a Si(III) oxidation state without progressing to the fully oxidized Si(IV) state. Second, this observation suggests that once a surface Si atom has its three Si−Si back-bonds oxidized, forming three Si−O−Si species, oxygen cannot readily insert into its fourth bond, the Si−C bond. Thus, while the first and second layer Si atoms may oxidize, oxygen cannot penetrate past the second layer Si, and vertical progression of the oxide into the bulk crystal is disrupted. Taken together, these observations suggest that the robustness of the surface Si−C bond is likely the key to halting the supply of O atoms to the bulk crystal and halting the vertical propagation of the native silicon oxide layer.

The above mechanistic considerations alone do not address the slow observed rate of oxidation of the topmost and second layers of Si atoms on the alkylated surfaces. The data indicate that such oxidation is significantly inhibited by alkylation even with use of alkyl groups that cannot sterically cover every Si atom site. Hence, lateral oxide growth and propagation is inhibited by even a partial coverage of Si−C bonds. If lateral propagation of oxide growth required adjacent Si−H atop sites on the Si surface, then even a partial coverage of Si−C alkyl bonds would be sufficient to significantly inhibit the surface oxidation, in accord with the observations. A purely steric argument of preventing access of the reactants to the surface, such as has been observed for self-assembled monolayers of alkanethiols on Cu, is unlikely to account for the observations, since the rate of such reactant penetration would have to be inhibited by orders of magnitude even for ethyl groups on Si surfaces. However, ethyl groups do not show close packing or long-range order on Si(111) surfaces, as evidenced by atomic resolution scanning tunneling microscopy (STM) studies of H_5C_2-terminated Si(111) surfaces.[39]

Finally, even when oxide does eventually grow on alkylated Si(111) surfaces, the SAM data show that the oxide forms in discrete patches and striations. This behavior suggests that the initial sites of oxidation are along step edges, and that the oxidation propagates more readily in such regions than on the terraces (Figure 6). However, the degree of passivation of even the step edges must be significant because highly stepped, vicinal surfaces oxidized at a rate similar to surfaces with large terraces. This behavior indicates that even step edges and kink sites, or regions near such sites, must be largely passivated toward oxidation by the alkylation process. The nonuniform growth pattern suggests that the growth requires nucleation and propagation in the vicinity of relatively susceptible defect sites even on step edges, terraces, or kink sites, to allow for oxide growth and passivation laterally on the surface.

V. Conclusions

Surface-sensitive SXPS of Si(111) surfaces alkylated through a two-step chlorination/alkylation technique has been used to investigate the growth of native oxides on samples kept in ambient air. This alkylation technique drastically reduced the growth of silicon oxides over a period of at least 2 months, with $<$0.40 ML of silicon oxides formed over this time. The oxide that is observed is principally Si^+ and Si^{3+}, with very limited contributions from the other silicon suboxides that are seen on unpassivated Si surfaces exposed to the same ambient conditions. This effect was, to first order, identical for surfaces alkylated with both small CH_3− groups and with larger, bulkier C_2H_5− and $C_6H_5CH_2$− moieties which are not sterically able to fit on every surface Si atom. SAM investigations of the freshly prepared and oxidized C_2H_5-terminated Si(111) surface demonstrated that silicon oxides do not grow uniformly on the surface, but instead appear in small patches leaving the rest of the Si surface unoxidized. When the oxidation behavior of two surfaces of differing step edge density was evaluated, no difference in Si oxide growth was seen over a period of several weeks. An explanation for this behavior is that surface alkylation protects the step edges from oxidation, leaving the terraces to oxidize at the same slow rate on each alkylated surface.[24] Taken together, these observations suggest that replacement of surface Si−H or Si−Cl bonds by Si−C bonds fundamentally disrupts the mechanism of Si surface oxidation, not simply blocks the surface physically from ambient reactants.

Acknowledgment. We gratefully acknowledge the National Science Foundation for support of this work (grants CHE-0213589) and for providing a graduate research fellowship to L.J.W. A.C. acknowledges support from the Army Research Office. This research was carried out in part at the National Synchrotron Light Source, Brookhaven National Laboratory, which is supported by the U. S. Department of Energy, Division of Materials Sciences and Division of Chemical Sciences, under Contract No. DE-AC02-98CH10886. We thank Michael Sullivan for use of the N_2(g)-purged glovebox at the NSLS. The scanning Auger microscopy was sponsored by the Assistant Secretary for Energy Efficiency and Renewable Energy, Office of FreedomCAR and Vehicle Technologies, as part of the High Temperature Materials Laboratory User Program, Oak Ridge National Laboratory, managed by UT-Battelle, LLC, for the U. S. Department of Energy under contract number DE-AC05-00OR22725. We also thank Y. Chabal for sharing a preprint of his manuscript on the oxidation of silicon in air.

References and Notes

(1) Royea, W. J.; Juang, A.; Lewis, N. S. *Appl. Phys. Lett.* **2000**, *77*, 1988−1990.

(2) Yablonovitch, E.; Allara, D. L.; Chang, C. C.; Gmitter, T.; Bright, T. B. *Phys. Rev. Lett.* **1986**, *57*, 249−252.

(3) Bent, S. F. *Surf. Sci.* **2002**, *500*, 879−903.

(4) Bansal, A.; Li, X.; Yi, S. I.; Weinberg, W. H.; Lewis, N. S. *J. Phys. Chem. B* **2001**, *105*, 10266−10277.

(5) Webb, L. J.; Lewis, N. S. *J. Phys. Chem. B* **2003**, *107*, 5404−5412.

(6) Keister, J. W.; Rowe, J. E.; Kolodziej, J. J.; Niimi, H.; Tao, H. S.; Madey, T. E.; Lucovsky, G. *J. Vac. Sci. Technol. A* **1999**, *17*, 1250−1257.

(7) Seah, M. P. Quantification of AES and XPS. In *Practical Surface Analysis*, 2nd ed.; Briggs, D., Seah, M. P., Eds.; John Wiley & Sons: Chichester, 1990; Vol. 1; pp 201−255.

(8) Sze, S. M. *The Physics of Semiconductor Devices*, 2nd ed.; Wiley: New York, 1981.

(9) Pi, T. W.; Hong, I. H.; Cheng, C. P.; Wertheim, G. K. *J. Electron Spectrosc. Relat. Phenom.* **2000**, *107*, 163−176.

(10) Himpsel, F. J.; Meyerson, B. S.; McFeeley, F. R.; Morar, J. F.; Taleb-Ibrahimi, A.; Yarmoff, J. A. Core Level Spectroscopy at Silicon Surfaces and Interfaces. In *Proceedings of the 1988 Enrico Fermi School on Photoemission and Absorption Spectroscopy of Solids and Interfaces with Synchrotron Radiation*; North-Holland: Varenna, 1988; pp 203−236.

(11) Proctor, A.; Sherwood, P. M. A. *Anal. Chem.* **1982**, *54*, 13−19.

(12) Shirley, D. A. *Phys. Rev. B* **1972**, *5*, 4709−4714.

(13) Contini, G.; Turchini, S. *Comput. Phys. Commun.* **1996**, *94*, 49−52.

(14) Himpsel, F. J.; McFeeley, F. R.; Taleb-Ibrahimi, A.; Yarmoff, J. A.; Hollinger, G. *Phys. Rev. B.* **1988**, *38*, 6084−6096.

(15) Haber, J. A.; Lewis, N. S. *J. Phys. Chem. B* **2002**, *106*, 3639−3656.

(16) Sherwood, P. M. A. Data Analysis in XPS and AES. In *Practical Surface Analysis*; Briggs, D., Seah, M. P., Eds.; John Wiley & Sons Ltd: New York, 1990; Vol. 1, pp 555−586.

(17) Durbin, T. D.; Simpson, W. C.; Chakarian, V.; Shuh, D. K.; Varekamp, P. R.; Lo, C. W.; Yarmoff, J. A. *Surf. Sci.* **1994**, *316*, 257−266.

(18) Kanashima, T.; Maida, O.; Kohma, N.; Agata, M.; Yudate, S.; Ueno, M.; Okuyama, M.; Ohashi, H. *Jpn. J. Appl. Phys.* **2001**, *40*, 4195−4196.

(19) Hwang, D. S.; Yasuda, T.; Ikuta, K.; Yamasaki, S.; Tanaka, K. *Jpn. J. Appl. Phys.* **1998**, *37*, 4204−4208.

(20) Helms, C. R.; Poindexter, E. H. *Rep. Prog. Phys.* **1994**, *57*, 791−852.

(21) van Oostrom, A.; Augustus, L.; Habraken, F. H. P. M.; Kuiper, A. E. T. *J. Vac. Sci. Technol.* **1982**, *20*, 953−956.

(22) Webb, L. J.; Nemanick, E. J.; Biteen, J. S.; Knapp, D. W.; Michalak, D. J.; Traub, M. C.; Chan, A. S. Y.; Brunschwig, B. S.; Lewis, N. S. *J. Phys. Chem. B* **2005**, *109*, 3930−3937.

(23) Rivillon, S.; Chabal, Y. J.; Webb, L. J.; Michalak, D. J.; Lewis, N. S.; Halls, M. D.; Raghavachari, K. *J. Vac. Sci. Technol. A* **2005**, *23*, 1100−1106.

(24) Garcia, S. P.; Bao, H.; Manimaran, M.; Hines, M. A. *J. Phys. Chem. B* **2002**, *106*, 8258−8264.

(25) Yu, H.; Webb, L. J.; Ries, R. S.; Solares, S. D.; Goddard, W. A.; Heath, J. R.; Lewis, N. S. *J. Phys. Chem. B* **2005**, *109*, 671−674.

(26) Webb, L. J.; Rivillon, S.; Michalak, D. J.; Chabal, Y. J.; Lewis, N. S. *J. Phys. Chem. B* **2006**, *110*, 7349−7356.

(27) Frank, M. M.; Chabal, Y. J. 2005, manuscript in preparation.

(28) Zhang, X.; Chabal, Y. J.; Christman, S. B.; Chaban, E. E.; Garfunkel, E. *J. Vac. Sci. Technol. A* **2001**, *19*, 1725−1729.

(29) Tachibana, A.; Sakata, K.; Sato, T. *Jpn. J. Appl. Phys.* **1998**, *37*, 4493−4504.

(30) Ogawa, H.; Ishikawa, K.; Inomata, C.; Fujimura, S. *J. Appl. Phys.* **1996**, *79*, 472−477.

(31) Yasaka, T.; Takakura, M.; Sawara, K.; Uenaga, S.; Yasutake, H.; Miyazaki, S.; Hirose, M. *IEICE Trans. Electron*. **1992**, *E75-C*, 764−769.

(32) Ohishi, K.; Hattori, T. *Jpn. J. Appl. Phys.* **1994**, *33*, L675−L678.

(33) Niwano, M.; Kageyama, J.; Kurita, K.; Kinashi, K.; Takahashi, I.; Miyamoto, N. *J. Appl. Phys.* **1994**, *76*, 2157−2163.

(34) Takahasi, K.; Nohira, H.; Nakamura, T.; Ohmi, T.; Hattori, T. *Jpn. J. Appl. Phys.* **2001**, *40*, L68−L70.

(35) Grunthaner, P. J.; Hecht, M. H.; Grunthaner, F. J.; Johnson, N. M. *J. Appl. Phys.* **1987**, *61*, 629−638.

(36) Yamamoto, K.; Hasegawa, M. *J. Vac. Sci. Technol. B* **1994**, *12*, 2493−2499.

(37) Sugiyama, K.; Igarashi, T.; Moriki, K.; Nagasawa, Y.; Aoyama, T.; Sugino, R.; Ito, T.; Hattori, T. *Jpn. J. Appl. Phys.* **1990**, *29*, L2401−L2404.

(38) Hattori, T.; Aiba, T.; Iijima, E.; Okube, Y.; Nohira, H.; Tate, N.; Katayama, M. *Appl. Surf. Sci.* **1996**, *104/105*, 323−328.

(39) Yu, H.; Webb, L. J.; Solares, S. D.; Cao, P.; Goddard, W. A., III; Heath, J. R.; Lewis, N. S. *J. Phys. Chem. B* **2006**, in press.